INTERNATIONAL JOURNAL FOR NUMERICAL METHODS IN ENGINEERING
Int. J. Numer. Meth. Engng 2015; **104**:566–584
Published online 1 July 2015 in Wiley Online Library (wileyonlinelibrary.com). DOI: 10.1002/nme.4972

A three-field stabilized finite element method for fluid-structure interaction: elastic solid and rigid body limit

E. Hachem[1,*,†], S. Feghali[1], T. Coupez[1] and R. Codina[2]

[1]*Center for Material Forming (CEMEF), MINES ParisTech, UMR CNRS 7635, Sophia Antipolis, France*
[2]*Universitat Politècnica de Catalunya (UPC), Jordi Girona 1-3, 08034 Barcelona, Spain*

SUMMARY

We propose a full Eulerian framework for solving fluid-structure interaction (FSI) problems based on a unified formulation in which the FSIs are modelled by introducing an extra stress in the momentum equation. The obtained three-field velocity, pressure and stress system is solved using a stabilized finite element method. The key feature of this unified formulation is the ability to describe different kind of interactions between the fluid and the structure, which can be either elastic or a perfect rigid body, without the need of treating this last case via penalization. The level-set method combined with a dynamic anisotropic mesh adaptation is used to track the fluid-solid interface. Copyright © 2015 John Wiley & Sons, Ltd.

Received 12 March 2014; Revised 21 January 2015; Accepted 9 June 2015

KEY WORDS: fluid-structure interaction; Eulerian description; rigid body limit; stabilized finite element method; anisotropic mesh adaptation

1. INTRODUCTION

Fluid-structure interaction (FSI) describes a wide variety of industrial problems arising in mechanical engineering, civil engineering and biomechanics. In spite of the available computer performance and the actual maturity of computational fluid dynamics and computational structural dynamics, several key issues still prevent accurate FSI simulations.

Two main approaches for the simulation of FSI problems are still gaining attention lately: partitioned and monolithic approaches. The partitioned approaches allow the use of a specific solver for each domain. The fluid and the structure equations are alternatively integrated in time, and the interface conditions are enforced asynchronously. The difficulty remains in transferring the information between the codes.

Different schemes, weakly or strongly coupled, are used to ensure the coupling between the two phases. The weakly coupled approach requires one solution of either field per time step but it consequently affects the accuracy of the coupling conditions. The strongly coupled version requires sub-iterations [1–4]. Results in the literature show that the approach is accurate and efficient. However, some instabilities may occur depending on the ratio of the densities and the complexity of the geometry [5]. Alternatively, authors in [6] propose an immersed particle method able to handle complicated FSI problems including cracking and perforation.

Monolithic methods are still of interest because of their capability to treat the interaction of the fluid and the structure using a unified formulation [7–9]. In this case, there is no need to enforce the continuity at the interface, it is obtained naturally. One unique conservation equation is then used to describe both the solid and the fluid domains.

*Correspondence to: E. Hachem, Center for Material Forming (CEMEF), MINES ParisTech, UMR CNRS 7635, Sophia Antipolis, France.
†E-mail: elie.hachem@mines-paristech.fr

In this paper, we propose a new monolithic formulation where the complete problem is written in a fully Eulerian framework and the fluid and solid phases are separated by a level set function. The same approach was proposed in [10, 11]. However, only the interactions between the fluid and rigid bodies were addressed, and therefore, the present paper is an extension of this previous work to allow dealing with elastic bodies, accounting for their full dynamics. The formulation we present here is again based on the introduction of an extra stress in the momentum equation. This extra stress is then related to the appropriate deformation tensor in the solid domain, with two different roles. In the case of an elastic solid, the relationship between the stress and the deformation is directly given by the constitutive law, whereas in the case of a rigid body the extra stress acts as a Lagrange multiplier to enforce that the deformation be zero in the solid. Therefore, apart from allowing a unified treatment of the solid and the fluid, the distinctive feature of our approach is the possibility of dealing exactly with perfectly rigid bodies. We are not aware of any other method with this capability.

Only few attempts can be found in the literature that deal with a rigid and elastic body in a unified formulation. Zhang and co-workers [12] solve the FSI problem using an immersed smoothed FEM. The fluid mesh is used to evaluate the FSI forces exerted on the solid; largely deformable solids are treated, and the rigid bodies can be considered by simply having a relatively high Young's modulus. An adaptive, staggered-grid version of the immersed boundary method is applied in [13] to simulate FSI model of the aortic heart valve. The thin leaflets are described as immersed elastic boundaries, and the wall of the aortic root is described as a thick, semi-rigid elastic structure. A monolithic FSI framework is considered in [14] for incompressible flow. A traditional marker-and-cell (MAC) grid discretization of the fluid and a fully Lagrangian discretization of the structures are used. Other approaches correspond to fixed-mesh methods, such as the fixed-mesh ALE formulation introduced in [15] and applied in [16, 17] to FSI and fluid-rigid body interaction. Some monolithic FSI formulations also use a sort of level set function to represent the solid surface, as in [18–21], even if the way to state the problem is different to the one we propose and the rigid body limit cannot be exactly reproduced.

The main limitation of the approach we use is the need of having a Eulerian description of the solid behaviour, with the deformation expressed as a function of the stress. Of course, this limitation is common to all purely approaches to treat the solids using a Eulerian frame, as for example, in [18–24], just to mention some works closely related to what we propose. In order to avoid treating this difficulty in detail, which deserves a research on its own, the constitutive model we shall use in this work is the incompressible neo-Hookean behaviour. Its application in an Eulerian framework can be found, for example, in [25, 26]. Even though it is the simplest hyperelastic model, it has been used for example to model biological tissues in several cases and has numerous industrial applications. We will introduce some definitions and transformations needed to develop a fluid-elastic interaction in a Eulerian framework following [27, 28]. The constitutive law requires the left Cauchy–Green strain tensor (also called Finger tensor) written in terms of the displacement field. In order to solve a problem posed in terms of velocities, we present here a way to approximate this strain tensor using only the velocity field to be computed and known values of the displacement.

As in [11], the obtained three-field velocity, pressure and stress system will be solved using a variational multiscale method. We combine this approximation with anisotropic mesh adaptation to ensure accurate capturing of the discontinuities at the fluid-structure interface. Details of the method are described in [11] and will not be repeated here.

This paper is organized as follow. First, the governing equations for the fluid and the solid are given in Section 2. Section 3 is dedicated to present the unified Eulerian formulation. The stabilizing schemes from a variational multiscale point of view are described in Section 4. In Section 5, the numerical performance of the proposed method is demonstrated by means of 2D and 3D test cases. Comparisons with the literature are provided. Finally, Section 6 is dedicated to conclusions and future work.

DOI: 10.1002/nme

2. GOVERNING EQUATIONS

As the proposed approach is monolithic, a unique conservation equation will be solved on the whole domain, with a variation of the constitutive equation depending on the phase that should be modelled. We start in this section by presenting each system of equation separately.

Let $\Omega \subset \mathbb{R}^d$ be the spatial domain at time $t \in [0, T]$, where d is the space dimension. Let $\partial\Omega$ denote the boundary of Ω. The fluid domain, the solid domain and the interface will be Ω_f, Ω_s and Γ_im, respectively. They verify the following:

$$\overline{\Omega}_\mathrm{f} \cup \overline{\Omega}_\mathrm{s} = \overline{\Omega} \quad \text{and} \quad \overline{\Omega}_\mathrm{f} \cap \overline{\Omega}_\mathrm{s} = \Gamma_\mathrm{im}.$$

The dynamics of the flow are given by the classical incompressible Navier–Stokes equations:

$$\rho_\mathrm{f} \frac{\partial \mathbf{v}}{\partial t} + \rho_\mathrm{f} \mathbf{v} \cdot \nabla \mathbf{v} - \nabla \cdot (2\eta_\mathrm{f} \boldsymbol{\varepsilon}(\mathbf{v})) + \nabla p = \rho_\mathbf{f} \mathbf{f} \quad \text{in } \Omega_\mathrm{f}, \tag{1}$$

$$\nabla \cdot \mathbf{v} = 0 \quad \text{in } \Omega_\mathrm{f}, \tag{2}$$

where $\mathbf{v}$ is the velocity field, ρ_f is the fluid density, p is the pressure, $\boldsymbol{\varepsilon}(\mathbf{v}) = (\nabla \mathbf{v} +^T \nabla \mathbf{v})/2$ is the deformation-rate tensor and η_f is the dynamic viscosity. As usual, $\mathbf{v} \cdot \nabla \mathbf{v}|_j = v_i \partial_i v_j$, with $\partial_i \equiv \partial/\partial x_i$, $i, j = 1, ..., d$ (the summation convention is adopted), even though we will take the gradient of a vector field defined by $\nabla \mathbf{v}|_{ij} = \partial_j v_i$.

Equations (1) and(2) are subject to the boundary and initial conditions:

$$\mathbf{v} = \mathbf{v}_{\Gamma,\mathrm{f}} \quad \text{on } \partial\Omega_\mathrm{f} \setminus \Gamma_\mathrm{im},\ t > 0, \tag{3}$$

$$\mathbf{v} = \mathbf{v}_\mathrm{im} \quad \text{on } \Gamma_\mathrm{im},\ t > 0, \tag{4}$$

$$\boldsymbol{\sigma} \cdot \mathbf{n} = \mathbf{t}_\mathrm{im} \quad \text{on } \Gamma_\mathrm{im},\ t > 0, \tag{5}$$

$$\mathbf{v}(\mathbf{x}, 0) = \mathbf{v_0}(\mathbf{x}) \quad \text{in } \Omega_\mathrm{f}, \tag{6}$$

where $\mathbf{v}_{\Gamma,\mathrm{f}}$ is a given velocity boundary condition, $\mathbf{v}_\mathrm{im}$ is the velocity at the fluid-solid interface Γ_im (the boundary of the immersed body), $\mathbf{n}$ is the outward normal on the solid surface, $\mathbf{t}_\mathrm{im}$ the normal stress on this boundary and $\mathbf{v_0}(\mathbf{x})$ is a given initial condition. For simplicity, only Dirichlet-type boundary conditions will be considered on the exterior boundary. For incompressible flows, the divergence-free constraint (2) gives rise to the pressure in the fluid.

In what follows, we treat the solid also in an Eulerian framework. Let ρ_s be the solid density, $\mathbf{u}$ the displacement field and p the solid pressure (positive in compression). If $\mathbf{X}$ is the position vector of a solid particle at the initial configuration and $\mathbf{x}$ at the current one (at time t), let the trajectory of this particle be given by $\mathbf{x} = \mathbf{x}(\mathbf{X}, t)$. The deformation gradient tensor in material (Lagrangian) coordinates is given by

$$\mathbf{F}(\mathbf{X}, t) := \frac{\partial \mathbf{x}}{\partial \mathbf{X}} = \mathbf{I} + \frac{\partial \mathbf{u}}{\partial \mathbf{X}} =: \mathbf{I} + \nabla_\mathbf{X} \mathbf{u},$$

where $\mathbf{I}$ is the d-dimensional identity and it is assumed that $\mathbf{u} = \mathbf{u}(\mathbf{X}, t)$ is given in material coordinates, with respect to which the gradient $\nabla_\mathbf{X}$ is computed. If $\mathbf{X} = \mathbf{X}(\mathbf{x}, t)$ are the inverse of the equations of motion, the inverse of tensor $\mathbf{F}$ in spatial (Eulerian) coordinates is

$$\mathbf{F}^{-1}(\mathbf{x}, t) := \frac{\partial \mathbf{X}}{\partial \mathbf{x}} = \mathbf{I} - \frac{\partial \mathbf{u}}{\partial \mathbf{x}} =: \mathbf{I} - \nabla_\mathbf{x} \mathbf{u}, \tag{7}$$

where now it is assumed that $\mathbf{u} = \mathbf{u}(\mathbf{x}, t)$ is given in spatial coordinates, even if we use the same symbol as before. We will see later how to approximate $\mathbf{F}$ in spatial coordinates from (7). We will omit the subscript $\mathbf{x}$ in ∇, that is, $\nabla \equiv \nabla_\mathbf{x}$.

The constitutive law for an incompressible neo-Hookean material in spatial coordinates can now be written as

$$\boldsymbol{\sigma}_\mathrm{s} = -p\mathbf{I} + \boldsymbol{\tau}_\mathrm{s}, \quad \boldsymbol{\tau}_\mathrm{s} = 2\mu_\mathrm{s} \mathbf{L}_\mathrm{s}, \quad \mathbf{L}_\mathrm{s} := \frac{1}{2}(\mathbf{F} \cdot \mathbf{F}^t - \mathbf{I}), \tag{8}$$

DOI: 10.1002/nme

where μ_s is the Lamé coefficient, a material parameter, and $\mathbf{L}_s$ is a strain tensor computed with the left Cauchy–Green deformation tensor $\mathbf{B} = \mathbf{F} \cdot \mathbf{F}^t$.

The problem to be solved for the solid consists then in finding a displacement field $\mathbf{u}$, a velocity $\mathbf{v}$, a pressure p and a tensor of deviatoric stresses $\boldsymbol{\tau}_s$ solution to the equations:

$$\rho_s \left(\partial_t \mathbf{v} + \mathbf{v} \cdot \nabla \mathbf{v}\right) - \nabla \cdot \boldsymbol{\tau}_s + \nabla p = \mathbf{f} \quad \text{in } \Omega_s,\ t > 0, \tag{9}$$

$$\nabla \cdot \mathbf{v} = 0 \quad \text{in } \Omega_s,\ t > 0, \tag{10}$$

$$\mathbf{L}_s(\mathbf{u}) - \frac{1}{2\mu_s}\boldsymbol{\tau}_s = \mathbf{0} \quad \text{in } \Omega_s,\ t > 0, \tag{11}$$

$$\partial_t \mathbf{u} + \mathbf{v} \cdot \nabla \mathbf{u} = \mathbf{v} \quad \text{in } \Omega_s,\ t > 0.s \tag{12}$$

Remarks

- Instead of using the reationship between the displacement field and the velocity field given by (12), it is also possible to avoid the calculation of $\mathbf{u}$ by transporting directly the deformation gradient tensor $\mathbf{F}$, which requires to solve a transport equation for it. This is the strategy used, for example, in [25, 29].
- For incompressible materials, the Poisson ratio ν is $\frac{1}{2}$, and therefore, the expression that relates the Lamé coefficents μ_s to the Young modulus E reduces to
$$\mu_s = \frac{E}{2(1 + 0.5)} = \frac{E}{3}.$$
- The main objective of writing the problem as we have performed is to obtain a unified formulation capable of dealing with both elastic structures and the rigid body case. This can be performed using Equation (11). More precisely, if μ_s tends to infinity, then $\frac{1}{2\mu_s}\boldsymbol{\tau}_s$ tends to zero, which means also that $\mathbf{L}_s(\mathbf{u})$ tends to zero, and consequently, we recover to the rigid body case. Hence, if μ_s has a large value, Equation (11) can be solved using an augmented Lagrangian method coupled with an Uzawa scheme (see [10, 11] for details). Otherwise, the extra stress tensor $\boldsymbol{\tau}_s$ can be computed directly using this equation. The limit case $\mu_s = \infty$ can be exactly taken into account. It is important to note that then $\boldsymbol{\tau}_s$ only appears in the momentum conservation equation, acting as a Lagrange multiplier to enforce a rigid body motion.

Equations (9)–(12) are subject to the following boundary and initial conditions:

$$\mathbf{v} = \mathbf{v}_{\Gamma,s} \quad \text{on } \partial\Omega_s \setminus \Gamma_{im},\ t > 0, \tag{13}$$

$$\mathbf{v} = \mathbf{v}_{im} \quad \text{on } \Gamma_{im},\ t > 0, \tag{14}$$

$$\boldsymbol{\sigma} \cdot \mathbf{n} = -\mathbf{t}_{im} \quad \text{on } \Gamma_{im},\ t > 0, \tag{15}$$

$$\mathbf{v}(\mathbf{x}, 0) = \mathbf{v_0}(\mathbf{x}) \quad \text{in } \Omega_s. \tag{16}$$

3. UNIFIED EULERIAN FORMULATION

3.1. Interface description

The monolithic approaches impose the use of an appropriate constitutive equation describing both the fluid and the solid domain. This offers a great flexibility to deal with different shapes or to change easily the physical properties for each immersed structure. Therefore, we start by computing the signed distance function (level set) of a given geometry to each node of the mesh. Using the zero isovalue of this function, we can easily identify the fluid-solid interface. Consequently, different parts are immersed in a larger domain of different constitutive laws.

DOI: 10.1002/nme

At any point $\mathbf{x}$ of the computational domain Ω, the level-set function α corresponds to the signed distance from Γ_{im}. In turn, the interface Γ_{im} is given by the zero isovalue of the function α:

$$\begin{aligned} \alpha(\mathbf{x}) &= \pm d(\mathbf{x}, \Gamma_{\text{im}}), \mathbf{x} \in \Omega, \\ \Gamma_{\text{im}} &= \{\mathbf{x}, \alpha(\mathbf{x}) = 0\}. \end{aligned} \tag{17}$$

In this paper, the following sign convention is used: $\alpha \geqslant 0$ inside the solid domain defined by the interface Γ_{im} and $\alpha \leqslant 0$ outside this domain. Further details about the algorithm used to compute the distance are available in [30]. It is also possible to use functions smoother than $d(\mathbf{x}, \Gamma_{\text{im}})$ away from Γ_{im} (for example, [31]).

As explained, the signed distance function is used to localize the interface of the immersed structure but it is also used to initialize the desirable properties on both sides of the latter. Indeed, for the elements crossed by the level-set functions, fluid-solid mixtures are used to determine the element effective properties. A Heaviside function $H(\alpha)$ is then defined as follows:

$$H(\alpha) = \begin{cases} 1 \text{ if } \alpha > 0 \\ 0 \text{ if } \alpha < 0 \end{cases} \tag{18}$$

In the numerical approximation of the problem, we will consider a partition of the computational domain Ω with a finite element mesh made by a collection of element $\{K\}$. Anisotropic mesh refinement will be a crucial ingredient of the formulation [10, 11, 32, 33].

The Heaviside function can be smoothed to obtain a better continuity at the interface [34] using the following expression:

$$H_\varepsilon(\alpha) = \begin{cases} 1 & \text{if } \alpha > \varepsilon \\ \dfrac{1}{2}\left(1 + \dfrac{\alpha}{\varepsilon} + \dfrac{1}{\pi}\sin\left(\dfrac{\pi\alpha}{\varepsilon}\right)\right) & \text{if } |\alpha| \leqslant \varepsilon \\ 0 & \text{if } \alpha < -\varepsilon \end{cases} \tag{19}$$

where ε is a small parameter such that $\varepsilon = O(h_{\text{im}})$, known as the interface thickness, and h_{im} is the mesh size in the normal direction to the interface. In the vicinity of the interface, it can be computed using the following expression:

$$h_{\text{im}} = \max_{j,l \in K} \nabla\alpha \cdot \mathbf{x}^{jl}, \tag{20}$$

where $\mathbf{x}^{jl} = \mathbf{x}^l - \mathbf{x}^j$ and K is the mesh element under consideration. According to the chosen approximations, the Heaviside function is then approximated using linear interpolations ($P1$) between fluid and solid properties or a piecewise constant interpolation ($P0$).

Finally, we combine this approach with an anisotropic mesh adaptation algorithm to ensure an accurate capturing of the discontinuities at the fluid-solid interface. However, the level-set function intersects the mesh element arbitrarily. It is possible then to overtake the discontinuity appearing at the interface by using mesh adaptation and regularization. The regularization parameter can be seen as the thickness or the resolution of the interface. It is shown that using local adaptivity, stretched elements at the interface are obtained, and one can then choose a priori the resolution of the thickness to be very small, which leads to very sharp interfaces, favourable for simulating FSIs. All the details on the used algorithm are explained in [32, 33].

3.2. Initial and boundary value problem

Now that each system is expressed in the Eulerian framework, we may combine Equations (1)–(6) and Equations (9)–(16) into one global system using the geometrical representation given by $H(\alpha)$ as follows:

DOI: 10.1002/nme

$$
\begin{aligned}
\rho\,(\partial_t \mathbf{v} + \mathbf{v}\cdot\nabla\mathbf{v}) - \nabla\cdot(2\eta\,\boldsymbol{\varepsilon}(\mathbf{v}) + \boldsymbol{\tau} - p\,\mathbf{I}) &= \mathbf{f} && \text{in } \Omega,\ t>0,\\
\nabla\cdot\mathbf{v} &= 0 && \text{in } \Omega,\ t>0,\\
\mathbf{L}(\mathbf{u}) - \frac{1}{2\mu_{\mathrm{s}}}\boldsymbol{\tau} &= \mathbf{0} && \text{in } \Omega,\ t>0,\\
\partial_t \mathbf{u} + \mathbf{v}\cdot\nabla\mathbf{u} &= \mathbf{v} && \text{in } \Omega_{\mathrm{s}},\ t>0,\\
\mathbf{v} &= \mathbf{v}_\Gamma && \text{on } \partial\Omega,\ t>0,\\
\mathbf{v}(\mathbf{x},0) &= \mathbf{v}_0(\mathbf{x}) && \text{in } \Omega,
\end{aligned}
\tag{21}
$$

where we have introduced

$$
\mathbf{v}_\Gamma = \begin{cases} \mathbf{v}_{\Gamma,\mathrm{s}} & \text{on } \partial\Omega_{\mathrm{s}}\cap\partial\Omega \\ \mathbf{v}_{\Gamma,\mathrm{f}} & \text{on } \partial\Omega_{\mathrm{f}}\cap\partial\Omega \end{cases}
$$

and

$$
\begin{aligned}
\mathbf{L}(\mathbf{u}) &= H(\alpha)\mathbf{L}_{\mathrm{s}}(\mathbf{u}),\\
\boldsymbol{\tau} &= H(\alpha)\boldsymbol{\tau}_{\mathrm{s}},\\
\eta &= (1-H(\alpha))\eta_{\mathrm{f}},\\
\rho &= \rho_{\mathrm{s}}H(\alpha) + \rho_{\mathrm{f}}(1-H(\alpha)).
\end{aligned}
$$

The boundary conditions (4)–(5) and (14)–(15) are then no longer needed.

It is observed that with the aid of $H(\alpha)$, we may use a single conservation equation to model both the fluid and the solid. The constitutive law incorporated in this conservation equation switches between that of the solid and that of the fluid depending solely on the value of $H(\alpha)$. Let us again note that inside the solid the stress $\boldsymbol{\tau}$ is a Lagrange multiplier to enforce $\mathbf{L}(\mathbf{u}) = \mathbf{0}$ when the solid is a rigid body. In [11], we used the condition $\boldsymbol{\varepsilon}(\mathbf{v}) = \mathbf{0}$ to characterize the rigid body motion, which is much simpler than imposing zero strain, $\mathbf{L} = \mathbf{0}$, because it does not require the introduction of the displacement field $\mathbf{u}$. However, this is now required if we want to consider also the possibility of dealing with an elastic solid.

3.3. Weak form

Let $V\times P\times\mathcal{T}\times U$ be the space where the unknowns $(\mathbf{v}, p, \boldsymbol{\tau}, \mathbf{u})$ are sought. The first and last spaces, V and U, are made of vector fields, which are square integrable in time with values in $H^1(\Omega)^d$ and satisfying the Dirichlet conditions. The second and third spaces, P and $\mathcal{T}$, are made of distributions in time with values in $P_0 = L^2(\Omega)/\mathbb{R}$ and $\mathcal{T}_0 = L^2(\Omega)^{d\times d}$, respectively (in fact, a subspace of $L^2(\Omega)^{d\times d}$ would be enough).

The corresponding test functions will be denoted $\mathbf{w}\in V_0 = H_0^1(\Omega)^d$, $q\in P_0$ and $\mathbf{z}\in U_0 = H_0^1(\Omega)^d$, $\boldsymbol{\xi}\in\mathcal{T}_0$. Multiplying by the test functions and integrating by parts, the associated standard weak form of system (21) can be stated as follows: find $\mathbf{v}\in V$, $p\in P$, $\boldsymbol{\tau}\in\mathcal{T}$ and $\mathbf{u}\in U$, satisfying the appropriate initial conditions and such that for all $t>0$

$$
\begin{aligned}
\rho(\partial_t\mathbf{v},\mathbf{w}) + \rho(\mathbf{v}\cdot\nabla\mathbf{v},\mathbf{w}) - (p,\nabla\cdot\mathbf{w}) + (2\eta\boldsymbol{\varepsilon}(\mathbf{v}),\boldsymbol{\varepsilon}(\mathbf{w})) + (\boldsymbol{\tau},\boldsymbol{\varepsilon}(\mathbf{w})) &= \langle\mathbf{f},\mathbf{w}\rangle,\\
(q,\nabla\cdot\mathbf{v}) &= 0,\\
-(\boldsymbol{\xi},\mathbf{L}(\mathbf{u})) + \frac{1}{2\mu_{\mathrm{s}}}(\boldsymbol{\xi},\boldsymbol{\tau}) &= 0,\\
(\partial_t\mathbf{u},\mathbf{z}) + (\mathbf{v}\cdot\nabla\mathbf{u},\mathbf{z}) &= (\mathbf{v},\mathbf{z}),
\end{aligned}
\tag{22}
$$

for all $(\mathbf{w}, q, \boldsymbol{\xi}, \mathbf{z})\in V_0\times P_0\times\mathcal{T}_0\times U_0$. Here and in the succeeding sections, $(\cdot,\cdot)$ stands for the standard L^2 product of two functions. Abusing of the notation, we will use the same symbol when the two functions are not necessarily in L^2. The duality between the velocity test functions and the external forces is denoted by $\langle\cdot,\cdot\rangle$.

DOI: 10.1002/nme

4. STABILIZED FINITE-ELEMENT METHOD

In this section, we describe the finite element approximation of the system of equations (22). Note that once discretized in time (see succeeding section), the displacement equation in (22) can be solved separately using a classical stabilized FEM, namely, the streamline upwind Petrov–Galerkin (SUPG) formulation. Therefore, only the three-field stabilized FEM corresponding to the first three equations in (22) will be detailed in this section.

4.1. Time discretization and approximation of the deformation gradient tensor

Any time discretization of the variational problem given by (22) is in principle possible. To fix ideas, we will consider a backward differencing (BDF) finite difference scheme in time with a constant time step δt. In this case, the temporal derivative of a function f is approximated by a difference formula $\delta_t f$ involving the values of f at the time step of interest as well as values in previous time steps. Because there is no possibility of confusion, no superscript will be used for the unknowns to be computed at a certain time step.

Let us describe now a way to approximate tensor $\mathbf{F}$ using the velocity field to be computed, $\mathbf{v}$, and the displacement field computed in the previous time step, $\mathbf{u}$. Suppose that $\delta\mathbf{u}$ is the displacement increment in one time step, which we may approximate by $\delta\mathbf{u} \approx \delta t\,\mathbf{v}$ to second order, for example. Let $\mathbf{j} := \nabla\mathbf{u}$ and $\delta\mathbf{j} := \nabla\delta\mathbf{u}$, where gradients are computed with respect to the Eulerian coordinates $\mathbf{x}$. We have that

$$\begin{aligned}\mathbf{F}(\mathbf{u}+\delta\mathbf{u}) &= (\mathbf{I}-\mathbf{j}-\delta\mathbf{j})^{-1}\\ &= [(\mathbf{I}-\mathbf{j})\cdot(\mathbf{I}-(\mathbf{I}-\mathbf{j})^{-1}\cdot\delta\mathbf{j})]^{-1}\\ &= (\mathbf{I}-\mathbf{F}(\mathbf{u})\cdot\delta\mathbf{j})^{-1}\cdot\mathbf{F}(\mathbf{u}).\end{aligned} \tag{23}$$

Now, we can expand this approximation to any order in $\delta\mathbf{j}$, which depends on the approximation order of the time integration schemes being used. Considering that $\mathcal{O}(|\delta\mathbf{j}|) = \mathcal{O}(\delta t)$, we may use, for example, the expansion

$$\mathbf{F}(\mathbf{u}+\delta\mathbf{u}) = \mathbf{F}(\mathbf{u}) + \mathbf{F}(\mathbf{u})\cdot\delta\mathbf{j}\cdot\mathbf{F}(\mathbf{u}) + (\mathbf{F}(\mathbf{u})\cdot\delta\mathbf{j})^2\cdot\mathbf{F}(\mathbf{u}) + \mathcal{O}(\delta t^3).$$

In the numerical examples, we will use a relatively simpler expression that may be obtained assuming that the strains are relatively small, so that cubic terms can be neglected. We may approximate the deformation gradient tensor by

$$\mathbf{F}(\mathbf{u}) = (\mathbf{I}-\mathbf{j})^{-1} \approx \mathbf{I}+\mathbf{j}+\mathbf{j}\cdot\mathbf{j},$$

in which we have neglected third order terms in $\mathbf{j}$. From this, we may approximate tensor $\mathbf{L}_s(\mathbf{u})$ by

$$\begin{aligned}2\mathbf{L}_s(\mathbf{u}) &= \mathbf{F}(\mathbf{u})\cdot\mathbf{F}(\mathbf{u})^t - \mathbf{I}\\ &\approx \mathbf{j}+\mathbf{j}\cdot\mathbf{j}+\mathbf{j}^t+\mathbf{j}\cdot\mathbf{j}^t+\mathbf{j}^t\cdot\mathbf{j}^t.\end{aligned}$$

Neglecting now quadratic terms in $\delta\mathbf{j}$, we may approximate

$$\begin{aligned}2\mathbf{L}_s(\mathbf{u}+\delta\mathbf{u}) &\approx \mathbf{j}+\delta\mathbf{j}+\mathbf{j}\cdot\mathbf{j}+\mathbf{j}\cdot\delta\mathbf{j}+\delta\mathbf{j}\cdot\mathbf{j}\\ &\quad+\mathbf{j}^t+\delta\mathbf{j}^t+\mathbf{j}\cdot\mathbf{j}^t+\mathbf{j}\cdot\delta\mathbf{j}^t+\delta\mathbf{j}\cdot\mathbf{j}^t+\mathbf{j}^t\cdot\mathbf{j}^t+\mathbf{j}^t\cdot\delta\mathbf{j}^t+\delta\mathbf{j}^t\cdot\mathbf{j}^t\\ &= 2\mathbf{L}_s(\mathbf{u})+\delta\mathbf{j}+\delta\mathbf{j}^t\\ &\quad+\mathbf{j}\cdot\delta\mathbf{j}+\delta\mathbf{j}\cdot\mathbf{j}+\mathbf{j}\cdot\delta\mathbf{j}^t+\delta\mathbf{j}\cdot\mathbf{j}^t+\mathbf{j}^t\cdot\delta\mathbf{j}^t+\delta\mathbf{j}^t\cdot\mathbf{j}^t,\end{aligned}$$

from where it follows that

$$\mathbf{L}_s(\mathbf{u}+\delta\mathbf{u}) \approx \mathbf{L}_s(\mathbf{u}) + \boldsymbol{\varepsilon}(\delta\mathbf{u}) + \mathbf{j}\cdot\boldsymbol{\varepsilon}(\delta\mathbf{u}) + \delta\mathbf{j}\cdot\boldsymbol{\varepsilon}(\mathbf{u}) + \frac{1}{2}\left(\mathbf{j}^t\cdot\delta\mathbf{j}^t+\delta\mathbf{j}^t\cdot\mathbf{j}^t\right).$$

Using the approximation $\delta\mathbf{u} \approx \delta t\,\mathbf{v}$, the strain tensor $\mathbf{L}$ can be finally expressed as

$$\mathbf{L}(\mathbf{u}+\delta\mathbf{u}) \approx \mathbf{L}(\mathbf{u}) + H(\alpha)\delta t\left[\boldsymbol{\varepsilon}(\mathbf{v}) + \nabla\mathbf{u}\cdot\boldsymbol{\varepsilon}(\mathbf{v}) + \nabla\mathbf{v}\cdot\boldsymbol{\varepsilon}(\mathbf{u}) + \frac{1}{2}(\nabla\mathbf{u}^t\cdot\nabla\mathbf{v}^t + \nabla\mathbf{v}^t\cdot\nabla\mathbf{u}^t)\right]. \tag{24}$$

DOI: 10.1002/nme

This approximation has been found to give accurate results in the numerical examples presented in this work. A formulation valid in a wider spectrum of problems should be based on the general equation (23), which should be employed in particular if more general constitutive laws than the one used in this work are needed. As mentioned earlier, we shall not touch this point, which is a general difficulty of constitutive laws for solids expressed in Eulerian references.

4.2. Multiscale approach

Let $\mathcal{K}_h = \{K\}$ be a finite element partition of Ω. From this, we may construct the finite dimensional approximation spaces for the velocity, the pressure and the stress that we denote by V_h, P_h and $\mathcal{T}_h$, respectively.

As it is well-known, the stability of the discrete formulation depends on appropriate compatibility restrictions on the choice of the finite element spaces. According to this, standard Galerkin mixed elements with, for example, continuous equal order linear/linear interpolation for the three fields are not stable. Lack of stability shows as uncontrollable oscillations that pollute the solution. We propose here a variational multiscale method, which allows one the use of equal order continuous interpolations for the three fields, apart from preventing from oscillations due to convection dominated flows. The basic idea is to consider that the unknowns can be split in two components, coarse and fine, corresponding to different scales or levels of resolution [35–38] First, we solve the fine scales in an approximate manner and then we replace their effect into the large scales.

Let us split the velocity, pressure and stress solution spaces as $V_h \oplus V'$, $P_h \oplus P'$ and $\mathcal{T}_h \oplus \mathcal{T}'$, respectively. Subscript h is used here, and in the following, to denote the finite element (coarse) component, whereas the prime is used for the so called subgrid scale (fine) component of the unknowns. It is understood now that these spaces correspond to the time discrete problem, even if we use the same notation as for the time continuous problem. According to this splitting, we have

$$\begin{aligned}
\mathbf{v} &= \mathbf{v}_h + \mathbf{v}' \ \in \ V_h \oplus V', \\
p &= p_h + p' \ \in \ P_h \oplus P', \\
\boldsymbol{\tau} &= \boldsymbol{\tau}_h + \boldsymbol{\tau}' \ \in \ \mathcal{T}_h, \oplus \mathcal{T}'
\end{aligned}$$

If the spaces for the test functions are split likewise, with a subscript 0 to identify them, problem (22) becomes: for each time step, find $(\mathbf{v}_h + \mathbf{v}', p_h + p', \boldsymbol{\tau}_h + \boldsymbol{\tau}') \in V_h \oplus V' \times P_h \oplus P' \times \mathcal{T}_h \oplus \mathcal{T}'$ such that

$$\begin{aligned}
&\rho(\delta_t(\mathbf{v}_h + \mathbf{v}'), \mathbf{w}_h + \mathbf{w}') + \rho((\mathbf{v}_h + \mathbf{v}') \cdot \nabla(\mathbf{v}_h + \mathbf{v}'), \mathbf{w}_h + \mathbf{w}') \\
&\quad - (p_h + p', \nabla \cdot (\mathbf{w}_h + \mathbf{w}')) + 2(\eta \boldsymbol{\varepsilon}(\mathbf{v}_h + \mathbf{v}'), \boldsymbol{\varepsilon}(\mathbf{w}_h + \mathbf{w}')) \\
&\quad + (\boldsymbol{\tau}_h + \boldsymbol{\tau}', \boldsymbol{\varepsilon}(\mathbf{w}_h + \mathbf{w}')) = \langle \mathbf{f}, \mathbf{w}_h + \mathbf{w}' \rangle,
\end{aligned} \tag{25}$$

$$(q_h + q', \nabla \cdot (\mathbf{v}_h + \mathbf{v}')) = 0, \tag{26}$$

$$(\mathbf{L}(\mathbf{u} + \delta\mathbf{u}), \boldsymbol{\xi}_h + \boldsymbol{\xi}') - \frac{1}{2\mu_s}(\boldsymbol{\tau}_h + \boldsymbol{\tau}', \boldsymbol{\xi}_h + \boldsymbol{\xi}') = 0, \tag{27}$$

for all $(\mathbf{w}_h + \mathbf{w}', q_h + q', \boldsymbol{\xi}_h + \boldsymbol{\xi}') \in V_{h,0} \oplus V_0' \times P_{h,0} \oplus P_0' \times \mathcal{T}_{h,0} \oplus \mathcal{T}_0'$. In (27), $\mathbf{L}(\mathbf{u} + \delta\mathbf{u})$ is given in terms of $\mathbf{v} = \mathbf{v}_h + \mathbf{v}'$ by (24), with $\mathbf{u}$ known from the previous time step.

Even though the subgrid scales (or subscales) could be approximated without further assumptions and inserted into the previous equations [37], we will make use of some common approximations, as well as an approximation particular of this problem:

(i) The subscales are not tracked in time, therefore, quasi-static subscales are considered here. However, the subscale equations remain quasi time-dependent.
(ii) The convective velocity of the non-linear term may be approximated using only the large-scale component, so that $(\mathbf{v}_h + \mathbf{v}') \cdot \nabla(\mathbf{v}_h + \mathbf{v}') \approx \mathbf{v}_h \cdot \nabla(\mathbf{v}_h + \mathbf{v}')$. Moreover, this approximation can be performed also if the convective term is written as $\nabla \cdot (\mathbf{v}_h + \mathbf{v}') \otimes (\mathbf{v}_h + \mathbf{v}')$, which is relevant when integrating by parts the convective term.

DOI: 10.1002/nme

(iii) Terms involving subscales can be integrated by parts, and the subscales on the element boundaries neglected.
(iv) In (24), when replacing $\mathbf{v}$ by $\mathbf{v}_h + \mathbf{v}'$, the velocity subscales will be multiplied by δt. We will neglect the resulting terms, so that (27) only contains the finite element velocity $\mathbf{v}_h$ and not its subscale component $\mathbf{v}'$.

4.3. Coarse scale equations and approximation of the fine scales

The equations for the coarse scales are obtained taking the subscale test functions equal to zero. Doing this and using the previous assumptions, we obtain

$$\begin{aligned}\rho(\delta_t \mathbf{v}_h, \mathbf{w}_h) + \rho(\mathbf{v}_h \cdot \nabla \mathbf{v}_h, \mathbf{w}_h) - (p_h + p', \nabla \cdot \mathbf{w}_h) + 2(\eta \boldsymbol{\varepsilon}(\mathbf{v}_h), \boldsymbol{\varepsilon}(\mathbf{w}_h)) \\ + (\boldsymbol{\tau}_h + \boldsymbol{\tau}', \boldsymbol{\varepsilon}(\mathbf{w}_h)) + \sum_K (\mathbf{v}', -\rho \mathbf{v}_h \cdot \nabla \mathbf{w}_h - 2\eta \nabla \cdot \boldsymbol{\varepsilon}(\mathbf{w}_h))_K = \langle \mathbf{f}, \mathbf{w}_h \rangle,\end{aligned} \tag{28}$$

$$(q_h, \nabla \cdot \mathbf{v}_h) - \sum_K (\mathbf{v}', \nabla q_h)_K = 0, \tag{29}$$

$$(\mathbf{L}(\mathbf{u}_h + \delta \mathbf{u}_h), \boldsymbol{\xi}_h) - \frac{1}{2\mu_s}(\boldsymbol{\tau}_h + \boldsymbol{\tau}', \boldsymbol{\xi}_h) = 0, \tag{30}$$

for all $(\mathbf{w}_h, q_h, \boldsymbol{\xi}_h) \in V_{h,0} \times P_{h,0} \times \mathcal{T}_{h,0}$, where $\sum_K$ stands for the summation over all the elements of the finite element partition $\mathcal{K}_h$, $(\cdot,\cdot)_K$ denotes the L^2 product in each K and

$$\begin{aligned}\mathbf{L}(\mathbf{u}_h + \delta \mathbf{u}_h) = \mathbf{L}(\mathbf{u}_h) \\ + H(\alpha)\delta t \left[\boldsymbol{\varepsilon}(\mathbf{v}_h) + \nabla \mathbf{u}_h \cdot \boldsymbol{\varepsilon}(\mathbf{v}_h) + \nabla \mathbf{v}_h \cdot \boldsymbol{\varepsilon}(\mathbf{u}_h) + \frac{1}{2}\left(\nabla \mathbf{u}_h^t \cdot \nabla \mathbf{v}_h^t + \nabla \mathbf{v}_h^t \cdot \nabla \mathbf{u}_h^t \right) \right].\end{aligned} \tag{31}$$

In this expression, $\mathbf{u}_h$ comes from the finite element approximation of the last equation in (22), which can performed using the SUPG method as indicated earlier.

The problem for the fine scales is obtained taking $(\mathbf{w}_h, q_h, \boldsymbol{\xi}_h) = (\mathbf{0}, 0, \mathbf{0})$ in (25)-(27) and using approximations i)-iv) described earlier. Introducing the FE residuals

$$\begin{aligned}\mathcal{R}_v &= \mathbf{f} - \rho \delta_t \mathbf{v}_h - \rho \mathbf{v}_h \cdot \nabla \mathbf{v}_h - \nabla p_h + \nabla \cdot \boldsymbol{\tau}_h + \nabla \cdot (2\eta \boldsymbol{\varepsilon}(\mathbf{v}_h)), \\ \mathcal{R}_p &= -\nabla \cdot \mathbf{v}_h, \\ \mathcal{R}_\tau &= \mathbf{L}(\mathbf{u}_h + \delta \mathbf{u}_h) - \frac{1}{2\mu_s}\boldsymbol{\tau}_h,\end{aligned}$$

and using the same ideas as in [36, 39], it turns out that the subscales may be approximated within each element $K \in \mathcal{K}_h$ by

$$\mathbf{v}' = \alpha_v \Pi'_v(\mathcal{R}_v), \quad p' = \alpha_p \Pi'_p(\mathcal{R}_p) \text{ and } \quad \boldsymbol{\tau}' = \alpha_\tau \Pi'_\tau(\mathcal{R}_\tau),$$

where Π'_v, Π'_p and Π'_τ are the projections onto V', P' and $\mathcal{T}'$, respectively, and α_v, α_p and α_τ are the so-called stabilization parameters. The most common choice is to take the former as the identity when applied to finite element residuals [35, 36], and this is what we will perform here, although it is also possible to take them as the orthogonal projection to the FE space (see [39] and references therein). Referring to the stabilization parameters, we compute them within each element as

$$\alpha_v = \left[\left(\frac{c_1 \eta}{\rho h_K^2} \right)^2 + \left(\frac{c_2 \|\mathbf{v}_h\|_K}{h_K} \right)^2 \right]^{-1/2}, \tag{32}$$

$$\alpha_p = \left[\left(\frac{\eta}{\rho} \right)^2 + \left(\frac{c_2 \|\mathbf{v}_h\|_K h_K}{c_1} \right)^2 \right]^{1/2}, \tag{33}$$

DOI: 10.1002/nme

$$\alpha_\tau = c_3 \frac{h_K}{L} 2H(\alpha)\mu_s, \tag{34}$$

where h_K is the element size, L a characteristic length of the computational domain, $\|\mathbf{v}\|_K$ a characteristic norm of $\mathbf{v}_h$ (with the same units as $\mathbf{v}_h$) in element K and c_1, c_2 and c_3 are algorithmic constants. We take them as $c_1 = 4$, $c_2 = 2$ and $c_3 = 1$ for linear elements.

Remarks

- Very often, the time step size of the temporal discretization is included in the expression of α_v. This improves the convergence behaviour of the algorithm to deal with the non-linearity of the problem, but has several conceptual drawbacks, as explained in [40, 41]. In order to make α_v more uniform over the computational domain and, as a consequence, improve the behaviour of the scheme, we may modify it as explained in [11].
- The factor h_K/L in (34) improves convergence of stresses when equal interpolation is used for all variables [36, 42]. However, it is possible to take it out (that is to say, to take $L = h_K$) and obtain optimal convergence for velocity and pressure [39]. In this case, $c_3 < 1$ needs to be taken.
- For the linear elements used in the numerical examples, terms of the form $\nabla \cdot (2\eta\boldsymbol{\varepsilon}(\mathbf{w}_h))$ involving second derivatives within each element can be neglected.

4.4. Stabilized formulation

Inserting the expression for the subscales obtained in (28)–(30), we finally obtain the stabilized finite element problem we were seeking. It consists in finding $(\mathbf{v}_h, p_h, \boldsymbol{\tau}_h) \in V_h \times P_h \times \mathcal{T}_h$ such that

$$\begin{aligned}
&\rho(\delta_t \mathbf{v}_h, \mathbf{w}_h) + \rho(\mathbf{v}_h \cdot \nabla \mathbf{v}_h, \mathbf{w}_h) - (p_h, \nabla \cdot \mathbf{w}_h) + 2(\eta\boldsymbol{\varepsilon}(\mathbf{v}_h), \boldsymbol{\varepsilon}(\mathbf{w}_h)) + (\boldsymbol{\tau}_h, \boldsymbol{\varepsilon}(\mathbf{w}_h)) \\
&\quad + \sum_K \alpha_v(\rho\delta_t \mathbf{v}_h + \rho\mathbf{v}_h \cdot \nabla \mathbf{v}_h + \nabla p_h - \nabla \cdot \boldsymbol{\tau}_h - 2\eta\nabla \cdot \boldsymbol{\varepsilon}(\mathbf{v}_h), \rho\mathbf{v}_h \cdot \nabla \mathbf{w}_h + 2\eta\nabla \cdot \boldsymbol{\varepsilon}(\mathbf{w}_h))_K \\
&\quad + \sum_K \alpha_p(\nabla \cdot \mathbf{v}_h, \nabla \cdot \mathbf{w}_h)_K + \sum_K \alpha_\tau(\mathbf{L}(\mathbf{u}_h + \delta\mathbf{u}_h) - \frac{1}{2\mu_s}\boldsymbol{\tau}_h, \boldsymbol{\varepsilon}(\mathbf{w}_h))_K = \langle \mathbf{f}, \mathbf{w}_h \rangle \\
&\quad + \sum_K \alpha_v(\mathbf{f}, \rho\mathbf{v}_h \cdot \nabla \mathbf{w}_h + 2\eta\nabla \cdot \boldsymbol{\varepsilon}(\mathbf{w}_h))_K,
\end{aligned} \tag{35}$$

$$\begin{aligned}
&(q_h, \nabla \cdot \mathbf{v}_h) + \sum_K \alpha_v(\rho\delta_t \mathbf{v}_h + \rho\mathbf{v}_h \cdot \nabla \mathbf{v}_h + \nabla p_h - \nabla \cdot \boldsymbol{\tau}_h - 2\eta\nabla \cdot \boldsymbol{\varepsilon}(\mathbf{v}_h), \nabla q_h)_K \\
&\quad = \sum_K \alpha_v(\mathbf{f}, \nabla q_h)_K,
\end{aligned} \tag{36}$$

$$\sum_K \left(1 - c_3 \frac{h_K}{L}\right)(\mathbf{L}(\mathbf{u}_h + \delta\mathbf{u}_h), \boldsymbol{\xi}_h)_K - \frac{1}{2\mu_s} \sum_K \left(1 - c_3 \frac{h_K}{L}\right)(\boldsymbol{\tau}_h, \boldsymbol{\xi}_h)_K = 0, \tag{37}$$

for all $(\mathbf{w}_h, q_h, \boldsymbol{\xi}_h) \in V_{h,0} \times P_{h,0} \times \mathcal{T}_{h,0}$. We have assumed $\mathbf{f} \in L^2(K)^d$ for simplicity.

When compared with the Galerkin formulation (22), the proposed stabilized formulation involves additional integrals that are evaluated element-wise. These additional terms represent the effects of the subgrid scales and they are introduced in a consistent way to the Galerkin formulation. All of these terms enable: (1) to overcome the instability of the classical formulation arising in convection dominated flows; (2) to circumvent the inf-sup condition for the velocity, pressure and stress interpolations; and (3) to add additional stability due to the insertion of the extra stress tensor. Note that (37) reduces to the standard Galerkin equation when isotropic elements are used, but the stress subscale still contributes to (35).

DOI: 10.1002/nme

The analysis of the formulation presented is outside the scope of this paper. If fact, we are not aware of any result even at the continuous level for formulations similar to the one presented here. Let us only remark that for problem (35)–(37), it could be possible to add a term of the form

$$\sum_K \delta t \alpha_v (\mathcal{R}_v, \nabla \cdot \boldsymbol{\xi}_h)_K \tag{38}$$

to the left-hand-side of (37). When combined with the terms in (35) and (36), it allows one to obtain control on the the norm of $\rho \mathbf{v}_h \cdot \nabla \mathbf{v}_h + \nabla p_h - \nabla \cdot \boldsymbol{\tau}_h$ when the test functions are taken equal to the finite element unknowns. We have found useful to include the term (38) in the numerical examples. Note that consistency is preserved, because this term depends on the residual of the momentum equation, and therefore, it vanishes if the finite element solution is replaced by the exact one.

5. NUMERICAL RESULTS

In order to validate the proposed formulation, four test cases are presented in this section. The results obtained with the proposed approach are compared with those obtained either by other approaches that can be found in the literature. In all cases, units are assumed to be given in SI.

The implementation with which the results to be presented have been obtained is essentially the same as in [10, 11]. Thus, we will not discuss it here, but let us only remark that it is possible to compute the stress $\boldsymbol{\tau}_h$ in a segregated manner, thus reducing the computational cost. In particular, in the rigid body limit, it acts as a Lagrange multiplier and can be computed using an augmented Lagrange formulation together with an Uzawa scheme, as mentioned earlier.

5.1. Flow in a cavity with an elastic wall

We consider first a stationary example, the lid-driven cavity with an elastic bottom wall. The cavity domain is the $[0, 2] \times [0, 2]$ square, with a horizontal elastic wall located at a height 0.5, whereas the upper part is filled with a fluid. The problem setup is depicted in Figure 1. The fluid viscosity is $\eta_{\mathrm{f}} = 0.2$, and the solid constant μ_{s} is set to 1. The density of both fluid and solid is $\rho_{\mathrm{f}} = \rho_{\mathrm{s}} = 1$. We prescribed a non-slip boundary conditions on all the walls except on the top lid where we impose v_x using the following expression:

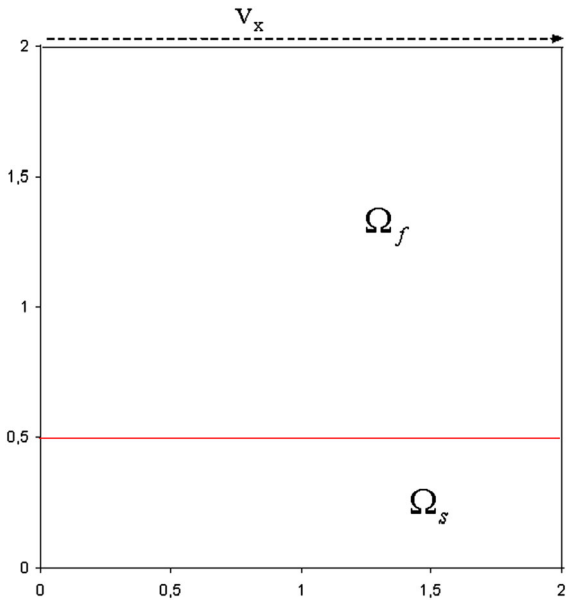

Figure 1. Schematic representation of the flow in a cavity with an elastic wall.

DOI: 10.1002/nme

$$v_x = 0.5 \begin{cases} 4x & x \in [0, 0.25] \\ 1 & x \in [0.25, 1.25] \\ 4(2-x) & x \in [1.75, 2] \end{cases} \tag{39}$$

We consider that the system reaches a steady state when the kinetic energy of the structure is below 10^{-8}. The velocity field and the comparison of the final and initial position of the interface are shown in Figure 2. The obtained result compares well with the solution reported in [18, 26].

Another similar test case can be found in Zhao *et al.* [43]. The domain is again a square, the lower half is a solid and the upper half is a fluid. A periodic vertical velocity is imposed at the top of the domain, given by

$$v_y = -\cos(2\pi t)\sin(2\pi x) \quad \text{and} \quad v_x = 0$$

Figure 3(a) shows the problem setup as described in [43]. The fluid viscosity is $\eta_f = 0.2$, and the solid has $\mu_s = 1$. The solid deforms because of the imposed fluid flow. Again, Figure 3 highlights a close agreement between our solution at time $t = 1$ and that reported in [43].

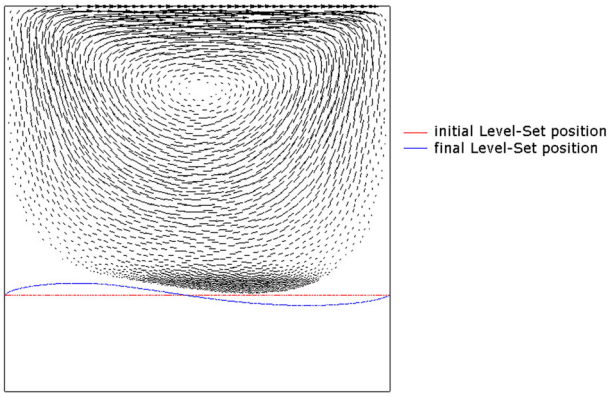

Figure 2. Velocity profile and the initial and final position of the interface.

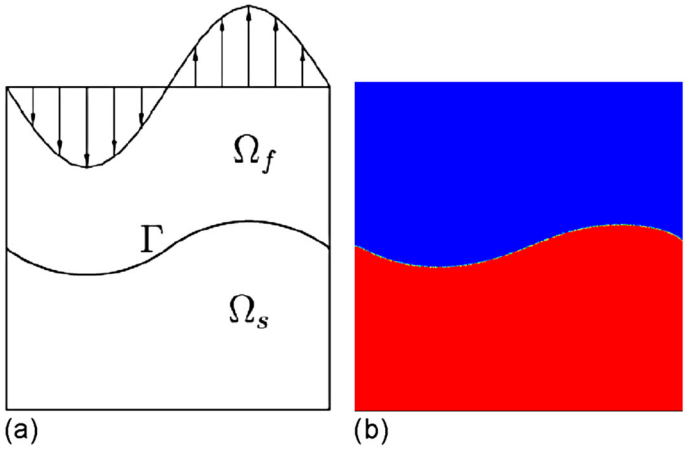

Figure 3. Deformation of an elastic solid driven by a fluid flow at time $t = 1$. (a) Schematic configuration and deformed solid given in [43]. (b) η distribution in the whole domain obtained with the formulation presented in this work.

DOI: 10.1002/nme

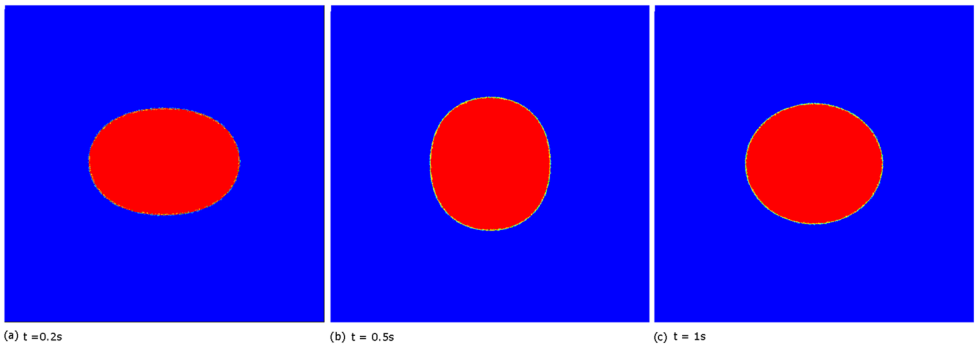

Figure 4. The evolution of the oscillating disk in time.

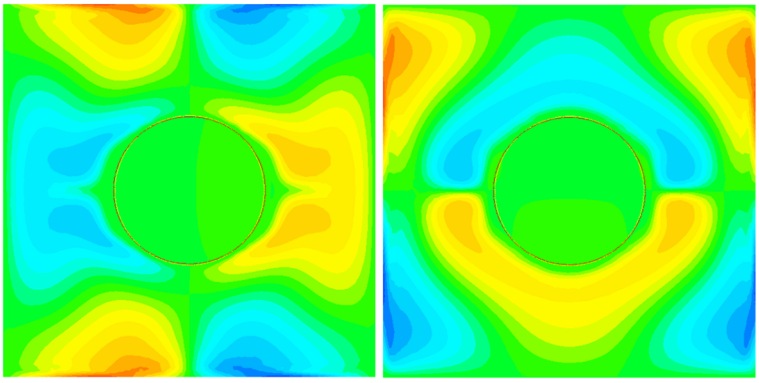

Figure 5. The displacement field in the x (left) and y (right) directions.

5.2. *Oscillating disk*

In this example, we study a 2D oscillating disk inside a cavity. The disk is placed at the center of a square cavity of side 1. A periodic boundary condition and an initial velocity are applied for both the fluid and the structure using the stream function:

$$\phi = \phi_0 \sin(k_x x) \sin(k_y y),$$

where $\phi_0 = 0.05$ and $k_x = k_y = 2\pi$.

A neo-Hookean constitutive model is considered for the structure with an elastic constant equal to 1. The structure and the fluid densities are set to $\rho_s = \rho_f = 1$. The dynamic viscosity of the fluid is set to $\eta_f = 0.001$. We performed the simulation for a period $T = 1$. Figures 4 and 5 show different snapshots of the oscillating disk and the displacement field taken at various time instances.

Solutions of this test case obtained in [14] showing the velocity profile and the structure deformation agree very well with our results in Figure 6.

The kinetic energy of the whole system is computed as follows:

$$E_k = \frac{1}{2} \int_\Omega |\mathbf{v}(\mathbf{x})|^2 d\mathbf{x}$$

The kinetic energy over time is plotted in Figure 7, showing a good agreement with the results reported in [14, 43].

5.3. *Elastic plate in an imposed flow*

In this example, a grid convergence study and error analysis are performed to assess the accuracy of the proposed formulation for a flexible plate in a 2D channel, as reported in [44]. The channel has length $L = 0.2$ and a height $H = 0.02$. The flexible plate is situated at the center of the channel, the length and height of the plate are 0.002 and 0.016, respectively. The model is depicted in Figure 8.

DOI: 10.1002/nme

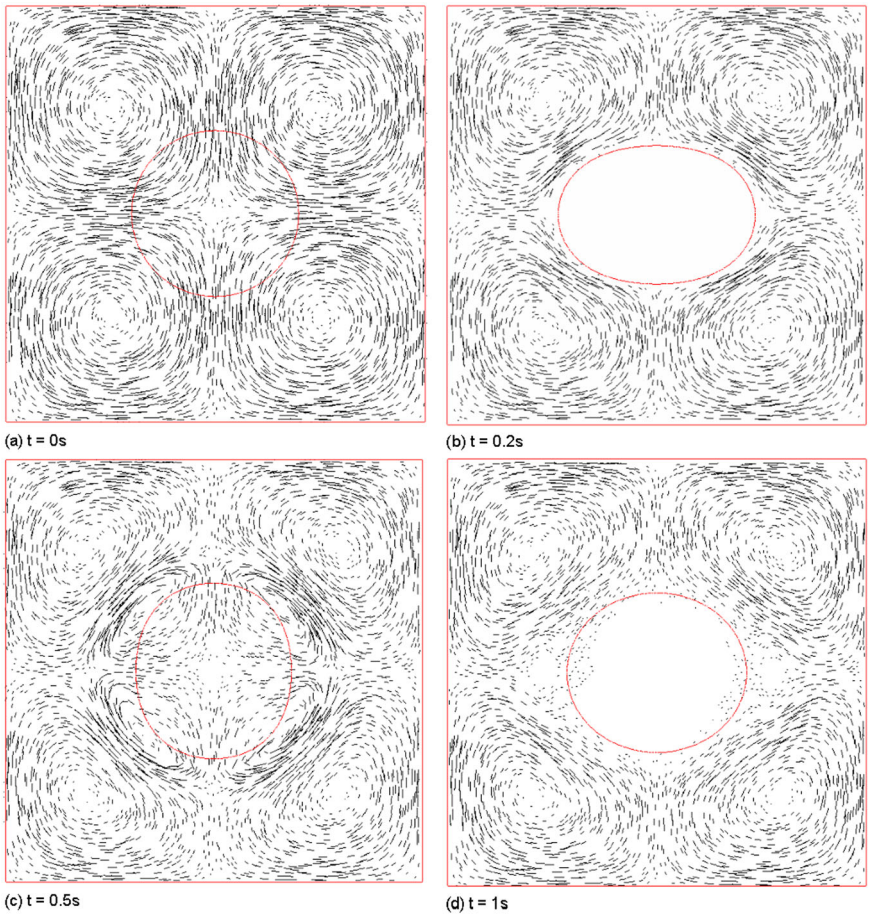

Figure 6. Velocity field around the oscillating disk at different time instants.

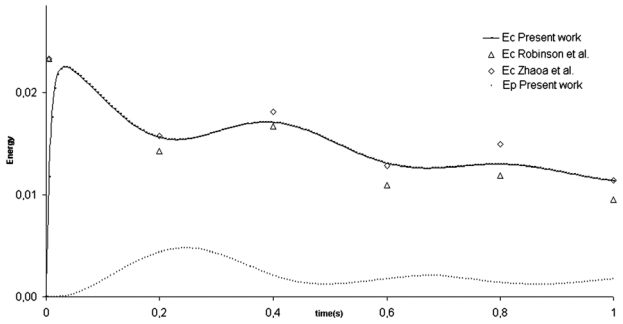

Figure 7. Comparisons of the kinetic energy evolution.

A sinusoidal velocity $v_x = 0.015\sin(2\pi t)$ is imposed at the inlet with a period $T = 1$. The fluid density and viscosity are $\rho_f = 1000$ and $\eta_f = 10^{-3}$, respectively. The structure is considered as an incompressible Neo-Hookean elastic material. Its density and Young's modulus are $\rho_s = 1000$ and $E = 5000$, respectively.

As in [44], and because there is no analytical solution to this problem, four unstructured meshes, with different mesh sizes, are used. The solution obtained using the finest mesh is considered as the reference solution. The four unstructured meshes used are named Mesh1, Mesh2, Mesh3 and Mesh4 with mesh sizes 0.002, 0.001, 0.0005 and 0.00025, respectively. Figure 9 shows that the geometric

DOI: 10.1002/nme

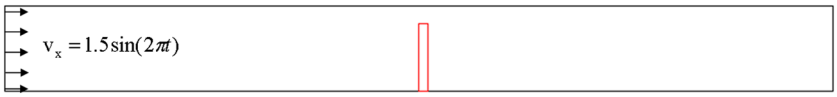

Figure 8. Schematic representation of a flexible plate in an imposed flow.

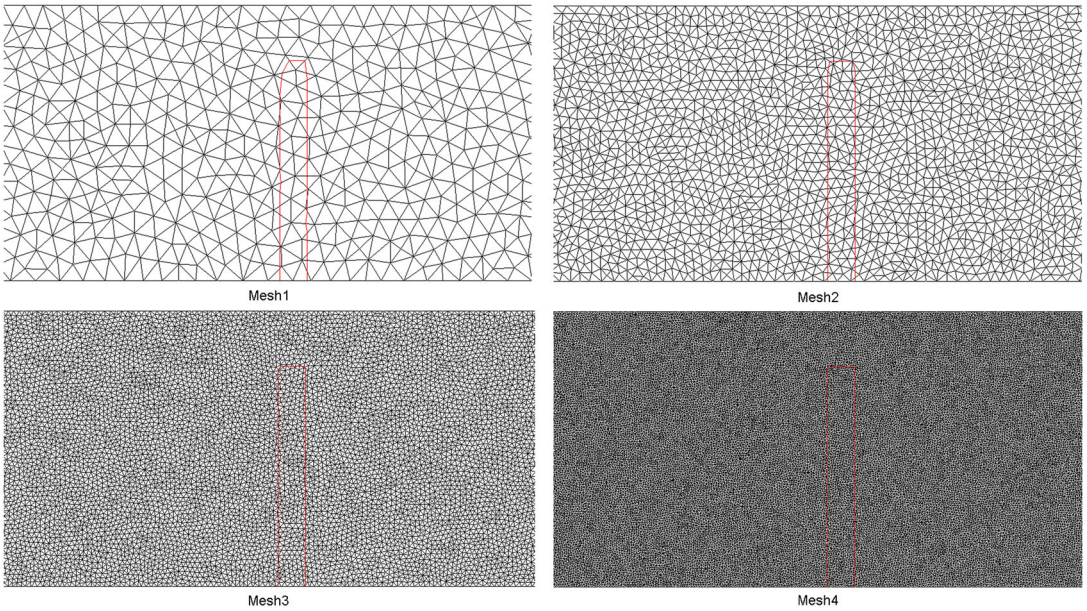

Figure 9. Four finer meshes used for grid convergence study and error analysis.

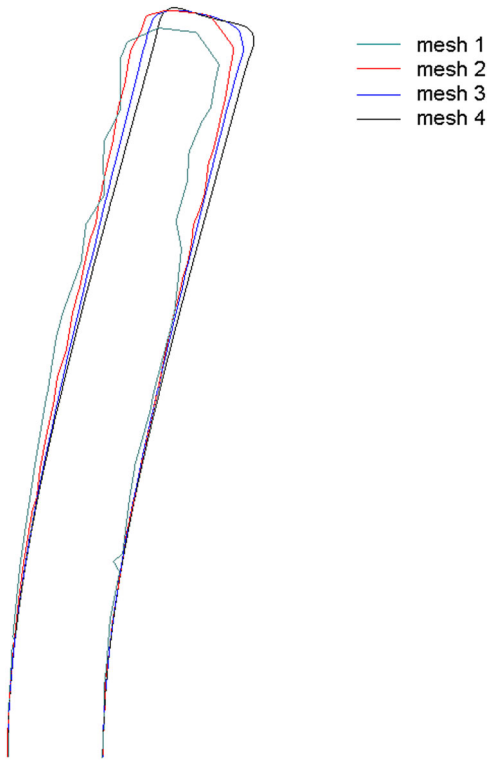

Figure 10. The zero isovalue of the level-set function at $t = 0.25$ obtained from the different meshes.

DOI: 10.1002/nme

representation of the elastic plate on Mesh1 is poor, revealing the importance of the mesh adaptation. Figure 10 shows the isovalue zero of the level-set functions obtained on each mesh at $t = 0.25$.

As expected, when the mesh is refined, the geometric representation becomes more precise, and the position of the structural interface tends to the one computed on the reference mesh. With anisotropic mesh adaptation, as proposed in Section 2, we may obtain a very accurate representation of the level-set function. However, in order to compare with results in [44] computed on structured meshes, we did not adapt the mesh in this test case and we used instead unstructured meshes. The errors are calculated for the displacement of the whole domain. The L^2 errors for the three meshes with respect to the finest one are depicted in Figure 11. The convergence rate of the L^2 errors is close to 2.

5.4. *Falling sphere in a channel*

We consider the problem of a single rigid sphere falling under gravity in a closed channel. Many test cases and convergence analysis on rigid body motion were studied in [11]. We repeated here a fluid-rigid interaction to highlight the capability of the proposed approach to deal with both elastic

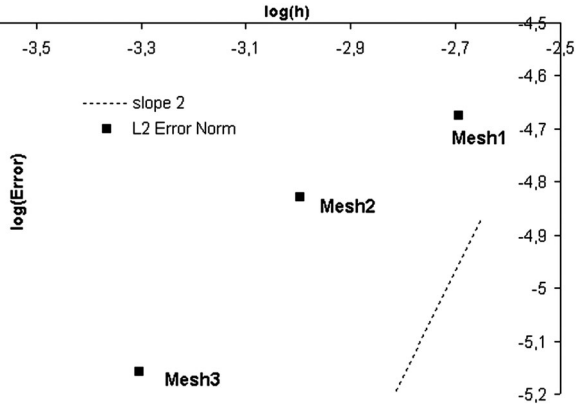

Figure 11. The L^2 errors for the three meshes with respect to the finest mesh.

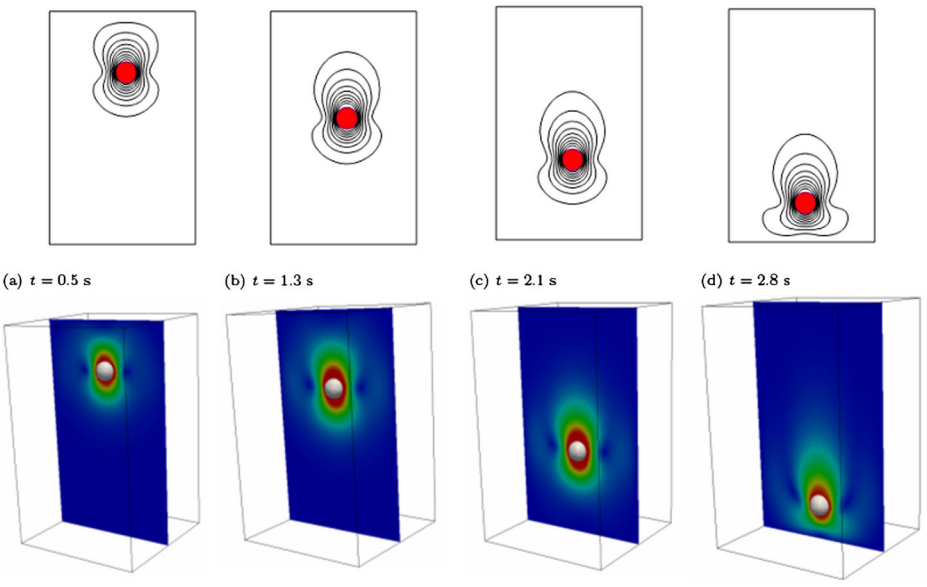

Figure 12. Contours of the velocity at different times during the fall: the reference [45] (top) and the present work (bottom).

DOI: 10.1002/nme

and rigid structures. The sphere has a density of $\rho_s = 1120$, a diameter of 0.015, initial position at height 0.12 and falling inside a channel of dimensions $0.1 \times 0.1 \times 0.16$. A non-slip boundary condition is applied on the walls. The fluid density and viscosity are set to $\rho_f = 970$ and $\eta_f = 3.73$, respectively. A fixed time step of $\delta t = 0.1$ is used. The mesh is unstructured and consists of 973 451 tetrahedral elements. The test case is inspired from [45].

Figure 12 shows very good agreement between our results and those in [45] for both the velocity and the position of the center of the disk with respect to time. This figure illustrates the velocity contours at selected times surrounding the zero isovalue of the disk level-set function. The agreement between the numerical solutions shows that the present approach is able to predict well the behaviour of the fluid even in the presence of a rigid body.

6. CONCLUSION

In this paper, we have described a stabilized three-field velocity-pressure-stress formulation for FSI problems, designed for cases involving elastic structures and rigid bodies immersed in an incompressible viscous flow. The proposed approach solves one set of equation in both domains with different constitutive laws, that is to say, the stress switches from that corresponding to a Newtonian fluid behaviour to that of an elastic or rigid body depending on the spatial point under consideration. In the latter case, this stress plays the role of a Lagrange multiplier to enforce zero strain in the solid region, whereas in the case of an elastic solid it is the classical Cauchy stress. Thus, one of the main features of the formulation proposed is the ability to deal with the rigid body motion exactly, and not as an approximation of this rigid body as an elastic solid with a very high stiffness.

Referring to the finite element approximation, the stabilized formulation employed allows one to use equal-order interpolation for the three fields, without the need to satisfy compatibility conditions between the spaces of stress and velocity on the one hand and between the pressure and velocity on the other hand. Moreover, we have devised approximations that have allowed us to pose the problem in such a way that the calculation of displacements in the solid can be segregated from the calculation of stress, velocity and pressure. The potential of the resulting formulation has been demonstrated in a set of numerical examples, in which we have obtained good accuracy and good numerical performance.

The natural extension of this work is to consider a different rheological behaviour for the solid. This extension is not necessarily straightforward. At the continuous level, it requires to write a certain deformation tensor in terms of the Cauchy stress to be inserted in the momentum equation written in a Eulerian framework. Numerically, one then has to be able to derive an approximation allowing to express the constitutive equation in terms of velocities and then design a stabilized finite element formulation of the resulting problem. Likewise, the analysis of the problem, both at the continuous and at the discrete level, is also an open issue.

ACKNOWLEDGEMENT

R. Codina gratefully acknowledges the financial support of the ICREA Acadèmia Program, from the Catalan Government.

REFERENCES

1. Le Tallec P, Mouro J. Fluid structure interaction with large structural displacements. *Computer Methods in Applied Mechanics and Engineering* 2001; **190**(24-25):3039–3067.
2. Fernández MA, Moubachir M. A Newton method using exact Jacobians for solving fluid-structure coupling. *Computers and Structure* 2005; **83**(2-3):127–142.
3. Gerbeau J-F, Vidrascu M. A quasi-Newton algorithm based on a reduced model for fluid structure interaction problems in blood flow. *Mathematical Modelling and Numerical Analysis* 2003; **37**:631–647.
4. Gerbeau J-F, Vidrascu M, Frey P. Fluid structure interaction in blood flows on geometries coming from medical imaging. *Computers and Structure* 2005; **83**(2-3):155–165.
5. Causin P, Gerbeau J-F, Nobile F. Added-mass effect in the design of partioned algorithms for fluid-structure problems. *Computer Methods in Applied Mechanics and Engineering* 2005; **194**:4506–4527.

DOI: 10.1002/nme

6. Rabczuk T, Gracie R, Song J-H, Belytschko T. Immersed particle method for fluid-structure interaction. *International Journal for Numerical Methods in Fluids* 2010; **81**:48–71.
7. Bathe KJ, Zhang H, Wang MH. Finite element analysis of incompressible and compressible fluid flows with free surfaces and structural interactions. *Computers and Structures* 1995; **56**:193–213.
8. Bathe KJ, Zhang H. A flow-condition-based interpolation finite element procedure for incompressible fluid flows. *Computers and Structures* 2002; **80**:1267–1277.
9. Michler C, van Brummelen E, Hulshoff S, de Borst R. A monolithic approach to fluid-structure interaction. *Computers and Fluids* 2004; **33**:839–848.
10. Feghali S, Hachem E, Coupez T. Monolithic stabilized finite element method for rigid body motions in the incompressible Navier-Stokes flow. *European Journal of Computational Mechanics* 2010; **19**(5–7):547–573.
11. Hachem E, Feghali S, Codina R, Coupez T. Immersed stress method for fluid structure interaction using anisotropic mesh adaptation. *International Journal for Numerical Methods in Engineering* 2013; **94**:805–825.
12. Zhang Z-Q, Liu GR, Khoo BC. Immersed smoothed finite element method for two dimensional fluid-structure interaction problems. *International Journal for Numerical Methods in Engineering* 2012; **90**(10):1097–0207.
13. Griffith B. Immersed boundary model of aortic heart valve dynamics with physiological driving and loading conditions. *International Journal for Numerical Methods in Biomedical Engineering* 2012:317–345.
14. Robinson A, Schroeder C, Fedkiw R. A symmetric positive definite formulation for monolithic fluid structure interaction. *Journal of Computational Physics* 2010; **230**(4):1547–1566.
15. Codina R, Houzeaux J, Coppola-Owen H, Baiges J. The fixed-mesh ALE approach for the numerical approximation of flows in moving domains. *Journal of Computational Physics* 2009; **228**:1591–1611.
16. Baiges J, Codina R. The Fixed-Mesh ALE approach applied to solid mechanics and fluid-structure interaction problems. *International Journal for Numerical Methods in Engineering* 2010; **81**:1529–1557.
17. Baiges J, Codina R, Coppola-Owen H. The Fixed-Mesh ALE approach for the numerical simulation of floating solids. *International Journal for Numerical Methods in Fluids* 2011; **67**:1004–1023.
18. He P, Qiao R. A full-Eulerian solid level set method for simulation of fluid-structure interactions. *Micro Fluid and Nano Fluid* 2011; **11**:557–567.
19. Cottet G-H, Maitre E, Milcent T. Eulerian formulation and level set models for incompressible fluid-structure interaction. *ESAIM: Mathematical Modelling and Numerical Analysis* 2008; **42**(3):471–492.
20. Richter T. A fully Eulerian formulation for fluid-structure-interaction problems. *Journal of Computational Physics* 2013; **233**:227–240.
21. Wick T. Fully Eulerian fluid-structure interaction for time dependent problems. *Computer Methods in Applied Mechanics and Engineering* 2013; **255**:14–26.
22. Duddu R, Lavier L, Hughes T, Calo V. A finite strain Eulerian formulation for compressible and nearly incompressible hyperelasticity using high-order B-spline finite elements. *International Journal for Numerical Methods in Engineering* 2012; **89**(6):762–785.
23. Fedkiw R, Aslam T, Merriman B, Osher S. A non-oscillatory eulerian approach to interfaces in multimaterial flows (the ghost fluid method). *Journal of Computational Physics* 1999; **152**:457–492.
24. Okazawa S, Kashiyama K, Kaneko Y. Eulerian formulation using stabilized finite element methods for large deformation solid dynamics. *International Journal for Numerical Methods in Engineering* 2007; **72**:1544–1559.
25. van Hoogstraten P, Slaats P, Baaijens F. An Eulerian approach to the finite element modelling of neo-Hookean rubber materials. *Applied Scientific Research* 1991; **48**:193–210.
26. Dunne T. An Eulerian approach to fluid-structure interaction and goal-oriented mesh adaptation. *International Journal for Numerical Methods in Fluids* 2006; **51**(9-10):1017–1039.
27. Bünisch S, Dunne TF, Rannacher R. *Numerics of Fluid-Structure Interaction*, Vol. 37. Birkhäuser: Basel, 2008.
28. Bost C. Méthodes level-set et pénalisation pour le calcul d'interaction fluide-structure. *Ph.D. Thesis*, Université Joseph Fourrier- Grenoble I, Grenoble, 2008.
29. Duddu R, Lavier L, Hughes T, Calo V. A finite strain Eulerian formulation for compressible and nearly incompressible hyperelasticity using high-order B-spline finite elements. *International Journal for Numerical Methods in Engineering* 2012; **89**:762–785.
30. Bruchon J, Digonnet H, Coupez T. Using a signed distance function for the simulation of metal forming processes: formulation of the contact condition and mesh adaptation. *International Journal for Numerical Methods in Engineering* 2009; **78**(8):980–1008.
31. Codina R, Soto O. A numerical model to track two-fluid interfaces based on a stabilized finite element method and the level set technique. *International Journal for Numerical Methods in Fluids* 2002; **40**:293–301.
32. Gruau C, Coupez T. 3D tetrahedral unstructured and anisotropic mesh generation with adaptation to natural and multidomain metric. *Computer Methods in Applied Mechanics and Engineering* 2006; **194**:4951–4976.
33. Coupez T. Génération de maillage et adaptation de maillage par optimisation locale. *Revue Européenne des Éléments Finis* 2000; **9**:403–423.
34. van der Pijl S, Segal A, Vuik C, Wesseling P. A mass-conserving level-set method for modelling of multi-phase flows. *International Journal for Numerical Methods in Fluids* 2005; **47**:339–361.
35. Hughes TRJ. Multiscale phenomena: Green's functions, the Dirichlet-to-Neumann formulation, subgrid scale models, bubbles and the origin of stabilized methods. *Computer Methods in Applied Mechanics and Engineering* 1995; **127**:387–401.
36. Badia S, Codina R. Stabilized continuous and discontinuous Galerkin techniques for Darcy flow. *Computer Methods in Applied Mechanics and Engineering* 2010; **199**:1654–1667.

DOI: 10.1002/nme

37. Codina R. Stabilized finite element approximation of transient incompressible flows using orthogonal subscales. *Computer Methods in Applied Mechanics and Engineering* 2002; **191**:4295–4321.
38. Hachem E, Rivaux B, Kloczko T, Digonnet H, Coupez T. Stabilized finite element method for incompressible flows with high Reynolds number. *Journal of Computational Physics* 2010; **229**(23):8643–8665.
39. Codina R. Finite element approximation of the three field formulation of the Stokes problem using arbitrary interpolations. *SIAM Journal on Numerical Analysis* 2009; **47**:699–718.
40. Codina R, Principe P, Guasch O, Badia S. Time dependent subscales in the stabilized finite element approximation of incompressible flow problems. *Computer Methods in Applied Mechanics and Engineering* 2007; **196**:2413–2430.
41. Badia S, Codina R. On a multiscale approach to the transient Stokes problem. Transient subscales and anisotropic space-time discretization. *Applied Mathematics and Computation* 2009; **207**:415–433.
42. Cervera M, Chiumenti M, Codina R. Mixed stabilized finite element methods in nonlinear solid mechanics: Part I: formulation. *Computer Methods in Applied Mechanics and Engineering* 2010; **199**:2559–2570.
43. Zhao H, Freunda J, Moser R. A fixed-mesh method for incompressible flow-structure systems with finite solid deformations. *Journal of Computational Physics* 2008; **227**(6):3114–3140.
44. Xia G, Lin C-L. An unstructured finite volume approach for structural dynamics in response to fluid motions. *Computers and Structures* 2008; **86**:684–701.
45. Sourabh V, Martin N, Patankar M. A numerical method for fully resolved simulation (frs) of rigid particle-flow interactions in complex flows. *Journal of Computational Physics* 2009; **228**:2712–2738.

DOI: 10.1002/nme